The Feasibility of Synthetic Computed Tomography (sCT) Generated from Magnetic Resonance for Calculating ATenuation (MRCAT) in Prostate Cancer for External Beam Radiotherapy Dose Calculation

ความเป็นไปได้ของการใช้งานภาพเอกซเรย์คอมพิวเตอร์สังเคราะห์ที่ได้จากภาพคลื่นแม่เหล็กไฟฟ้า คำนวณการลอดทอน (เอ็มอาร์แคท) สำหรับการคำนวณปริมาณรังสีด้วยเทคนิครังสีรักษาระยะไกลในมะเร็งต่อมลูกหมาก

Pronpawee Pudsena[1], Tanwiwat Jaikuna[2], Pitchayut Nakkrasae[2], Wisawa Phongprapun[2], Pittaya Dankulchai[2]

[1]Master degree of Science Program in Medical Physics, Faculty of Medical Siriraj Hospital, Mahidol University, Bangkok, Thailand

[2]Division of Radiation Oncology, Department of Radiology, Faculty of Medical Siriraj Hospital, Mahidol University, Bangkok, Thailand

Corresponding author

Pittaya Dankulchai

Division of Radiation Oncology, Department of Radiology, Faculty of Medical Siriraj Hospital, Mahidol University, Address: 2 Wang Lang Road, Siriraj, Bangkok Noi, Bangkok 10700

Email: pittaya.dan@mahidol.ac.th

พรปวีณ์ ปัดเสนา[1], แทนวิวัฒน์ ใจกุณา[2], พิชญุตม์ นาคกระแสร์[2], วิศวะ พงษ์ประพันธ์[2], พิทยา ด่านกุลชัย[2]

[1]หลักสูตรวิทยาศาสตรมหาบัณฑิต สาขาฟิสิกส์การแพทย์ ภาควิชารังสีวิทยา คณะแพทย์ศาสตร์ศิริราชพยาบาล มหาวิทยาลัยมหิดล กรุงเทพฯ ประเทศไทย

[2]สาขาวิชารังสีรักษา ภาควิชารังสีวิทยา คณะแพทย์ศาสตร์ศิริราชพยาบาล มหาวิทยาลัยมหิดล กรุงเทพฯ ประเทศไทย

ผู้นิพนธ์ประสานงาน

พิทยา ด่านกุลชัย

สาขาวิชารังสีรักษา ภาควิชารังสีวิทยา คณะแพทยศาสตร์ศิริราชพยาบาล มหาวิทยาลัยมหิดล กรุงเทพฯ ประเทศไทย

2 ถนนวังหลัง แขวงศิริราช เขตบางกอกน้อย กรุงเทพฯ 10700

อีเมล: pittaya.dan@mahidol.ac.th

Submitted: Nov 14, 2023

Revised: Dec 15, 2023

Accepted: Jan 2, 2024

Abstract

Background: Magnetic resonance (MR) image has recently become a trendy use for external beam radiotherapy (EBRT) dose calculation according to the dominance of high soft tissue contrast. However, the main challenge of applying an MR image for dose calculation is the lack of a correlation between the material's density and the computed tomography (CT) number in the MR image, which is mandatory for dose calculation in a commercial treatment planning system. Thus, synthetic CT (sCT) is introduced for EBRT dose calculation.

Objectives: This study aims to examine the feasibility of using MR image for Calculating A Ttenuation (MRCAT)-sCT imaging in prostate cancer patients to calculate the external beam dose.

Materials and methods: Ten prospective prostate cancer patients were enrolled in this study. The pCT and MR images were acquired using the pre-imaging protocol. Tumors and organs at risk (OARs) were delineated on planning CT (pCT) and sCT. The Hounsfield unit (HU) of each organ was compared between pCT and sCT. The volumetric modulated arc therapy (VMAT) plan was generated on pCT and calculated based on the Acuros XB (AXB) algorithm using Eclipse, then recalculated on sCT. The similarity between pCT- and sCT-based dose was evaluated using dosimetric data extracted from the dose-volume histogram and 3D gamma analysis.

Results: This study demonstrated a minor difference in HU between sCT and pCT in soft tissue (13.02±15.58 HU) while the discrimination of HU was larger in femur bone (51.59±49.08 HU). The mean HU of soft tissue in sCT was greater than in pCT; contrastingly, the mean HU of bone from sCT was lower than in pCT. The dose distributions calculated from sCT and pCT were similar (>95% gamma passing rate at all criteria (varies from 3%3mm to 1%1mm). Each dosimetric determination showed insignificant differences across all relevant contours.

Conclusion: MRCAT-generated sCT can calculate prostate cancer EBRT doses with a negligible dose difference from pCT. This study promotes prostate EBRT using MR-only workflow.

Keywords: MRCAT, MR-only planning, Prostate cancer, Synthetic CT

บทคัดย่อ

หลักการและเหตุผล: ภาพคลื่นแม่เหล็กไฟฟ้า (เอ็มอาร์) ถูกนำมาใช้ในการคำนวณปริมาณรังสีสำหรับรังสีรักษาระยะไกลมากขึ้น เนื่องจากสามารถแสดงความแตกต่างของเนื้อเยื่อได้ดี อย่างไรก็ตามการคำนวณปริมาณรังสีด้วยภาพเอ็มอาร์ยังขาดความสัมพันธ์ระหว่างความหนาแน่นวัสดุและเลขซีที ซึ่งจำเป็นต่อการคำนวณปริมาณรังสีในเครื่องวางแผนการรักษาเชิงพาณิชย์ ดังนั้นภาพซีทีสังเคราะห์จึงถูกพัฒนาและนำมาใช้ในการคำนวณปริมาณรังสีในรังสีรักษาระยะไกล

วัตถุประสงค์: เพื่อตรวจสอบความเป็นไปได้ในการใช้ภาพซีทีสังเคราะห์จากเอ็มอาร์แคทในการคำนวณปริมาณรังสีเทคนิครังสีรักษาระยะไกลสำหรับผู้ป่วยมะเร็งต่อมลูกหมาก

วัสดุและวิธีการ: ผู้ป่วยมะเร็งต่อมลูกหมาก จำนวน 10 ราย ได้รับการจำลองการรักษาโดยสร้างภาพซีทีและภาพซีทีสังเคราะห์โดยใช้โปรโตคอลก่อนการสร้างภาพ ขอบเขตรอยโรคและอวัยวะสำคัญใกล้เคียงถูกกำหนดบนภาพซีทีและภาพซีทีสังเคราะห์ แล้วทำการเปรียบเทียบเลขซีทีของแต่ละอวัยวะระหว่างค่าที่ได้จากภาพซีทีสังเคราะห์และภาพซีที ภาพแผนการรักษาเทคนิคการฉายรังสีแบบปรับความเข้มหมุนรอบตัวถูกสร้างขึ้นโดยอาศัยภาพซีที ปริมาณรังสีถูกคำนวณด้วยอัลกอริทึม Acuros XB ด้วยเครื่องวางแผนการรักษา Eclipse (เวอร์ชั่น 16.1) จากนั้นแผนการรักษาถูกถ่ายโอนและทำการคำนวณปริมาณรังสีใหม่โดยอาศัยภาพซีทีสังเคราะห์ ความเหมือนของการกระจายรังสีระหว่างการคำนวณโดยอาศัยภาพซีทีและภาพซีทีสังเคราะห์ถูกประเมินด้วยพารามิเตอร์ของปริมาณรังสี และการวิเคราะห์แกมมาแบบ 3 มิติ

ผลการศึกษา: เลขซีทีระหว่างภาพซีทีสังเคราะห์และภาพซีทีมีความแตกต่างกันเล็กน้อยในบริเวณเนื้อเยื่อ (13.02 ± 15.58 HU) และมีความแตกต่างกันเพิ่มมากขึ้นในกระดูกโคนขา (51.59 ± 49.08 HU) โดยเลขซีทีในภาพซีทีสังเคราะห์มีค่าสูงกว่าภาพซีทีในบริเวณเนื้อเยื่อและต่ำกว่าในบริเวณกระดูก การกระจายรังสีที่ได้จากการคำนวณโดยอาศัยภาพทั้งสองมีความคล้ายคลึงกัน (อัตราผ่านค่าแกมมา >95% ทุกเกณฑ์พิจารณา) และไม่พบความแตกต่างเมื่อพิจารณาค่าพารามิเตอร์ของปริมาณรังสีในอวัยวะสำคัญใกล้เคียง

ข้อสรุป: ภาพซีทีสังเคราะห์ที่สร้างด้วยเอ็มอาร์แคทสามารถคำนวณการกระจายรังสีได้ไม่แตกต่างจากภาพซีที การศึกษานี้ส่งเสริมการนำภาพซีทีสังเคราะห์ด้วยเอ็มอาร์เท่านั้นมาใช้ในขั้นตอนการรักษาด้วยรังสีระยะไกลในผู้ป่วยมะเร็งต่อมลูกหมาก

คำสำคัญ: เอ็มอาร์แคท, การวางแผนการรักษาด้วยเอ็มอาร์เท่านั้น, มะเร็งต่อมลูกหมาก, ภาพซีทีสังเคราะห์

J Thai Assoc Radiat Oncol 2024; 30(1): R1 - R18

Introduction

Computed tomography (CT) is commonly the primary imaging modality utilized in radiotherapy (RT) planning workflows due to its capacity to provide electron density maps crucial for dose calculations. The high geometric fidelity of three-dimensional (3D) anatomy and tissue heterogeneity information allows the isodose distribution to be calculated for tumors as well as the surrounding normal tissue doses. However, CT images in low contrast of the grayscale region, e.g., pelvis and abdomen, may present difficulties in identifying tissue features, especially to separate tumors and normal organs in prostate cancer, which impairs the contouring accuracy[1]. This difficulty of contouring in low contrast CT could lead to consecutive systematic uncertainty in radiotherapy workflow[2, 3].

The magnetic resonance (MR) image showed a superior advantage of contouring accuracy for the low contrast of the grayscale region[4, 5]. The tumors burden could be easily identified and separated from normal tissue in the tumors-invasion area. In addition, some MR imaging techniques provide a functional characteristic of tissue which promotes biological target contouring and the zone of highly condensed tumors cells[6]. Due to the advantage of MR over CT images, many publications aim to introduce MR in routine RT workflow, for example, using MR images for contouring, guiding the patient's setup, and tracking tumors or organs at risk before and during irradiation[7-9]. These approaches are accomplished through the process of image registration between CT and MR images. However, employing MR images for external beam radiotherapy (EBRT) dose calculations remains challenging, primarily due to the absence of essential electron density information. Consequently, the use of synthetic CT (sCT) derived from MR images has been proposed as a solution for EBRT dose calculations[10, 11].

There are many techniques for the sCT generation from MR images. The vast majority of approaches to sCT generation involve applying the derived Hounsfield unit (HU) from the planning CT (pCT), either personal or average values of an entire cohort, to the MR image. The bulk density override technique is one example of the HU transformation from CT to the MR image. The target regions of interest (ROIs) on the MR image were overridden by an average of relative or physical electron density extracted from ROIs on the pCT[12]. Another technique is mapping HU from the CT image directly to the MR image in the voxel-based technique[13-15].

Although the sCT is able to be generated by the transformation of HU, in many cases the accuracy of HU transformation still needs extensive verification in individual patients because it is strongly dependent on the accuracy of image registration between CT and MR. An enormous error could be seen in the

movable- and deformable-organs, e.g., the pelvis region, as the shape and volume of the bladder and rectum could move and change during the intra- and inter-scanning time. Moreover, a significant registration mismatch could be induced by setup uncertainty from the repositioning of the patient between CT and MR acquisition. In addition, several studies have investigated the impact of image registration between CT and MR and found that the uncertainty of cross-registration between both images could be around 2-4 mm[16-18]. This uncertainty in turn affects the accuracy of dose calculation based on the sCT.

Recently, a commercial MR for Calculating ATtenuation (MRCAT) solution is software that includes an option to generate the sCT. This function is available in the MRCAT solution sCT version 4.1 (Philips Healthcare, Finland)[7, 11]. The MRCAT technique uses a dedicated MR sequence (a dual-echo 3D mDIXON fast field echo (FFE)) to generate the sCT and is valid for the MR-only clinical dose calculation in the brain, head and neck, and pelvis region. This technique is independent of image registration. However, the accuracy validation of the sCT before use in routine clinics is required.

This study aims to investigate the feasibility of the sCT generated from the MRCAT for prostate cancer by considering the accuracy of HU and dose calculation between the sCT and pCT at the Division of Radiation Oncology, Department of Radiology, Faculty of Medicine, Siriraj Hospital.

Materials and Methods

Patient Selection and Pre-imaging Preparation

Ten definitive radiotherapy prostate cancer patients were enrolled in this prospective study which was approved by the Siriraj Institutional Review Board (SIRB protocol No. 039/2565). The patients provided informed consent to acquire the additional mDIXON sequence during the MR scan and data collection. The data were collected from March to July 2022. This study was not include patients who had fiducial marker implantation and metal insertion in the pelvis region from surgery. As part of the pre-imaging process, all patients followed a protocol of consuming 600 ml of water after completed urination for full bladder condition, ensuring emptied rectum. Prior to the MR scan, CT imaging was performed approximately 40 minutes after water intake.

Image Acquisition

All patients underwent CT and MR imaging consecutively on the same date. The planning CT (pCT) and sCT-generated from the MR image was reconstructed and used for HU comparison of each organ and dose calculation, whereas the MR image was used for contouring purposes. Examples of the pCT and sCT for dose calculation and MR image for contouring purposes are shown in **Figure 1**. In this study, the controlling protocol of bladder dimension was established to maintain the size and shape of the bladder in all image modalities. The bladder dimensions

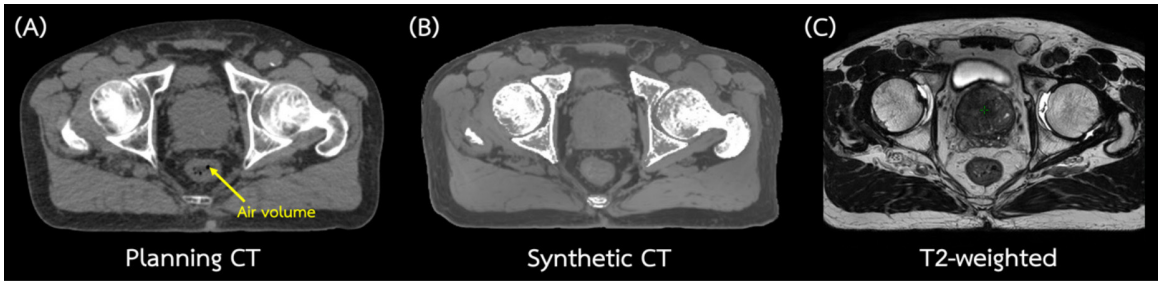

Figure 1. The different images on the same patient obtained from (A) pCT imaging, (B) sCT generating, and (C) MR imaging.

were measured from right-left (RL) of the bladder wall in the axial plane for the RL dimension, from mid-pubic symphysis to the mid-bladder dome for the craniocaudal (CC) dimension, and from anterior to posterior of the bladder wall in the midsagittal plane for the anteroposterior (AP) dimension. The bladder lengths from the pCT and MR images were collected and reported by a single observer to eliminate inter-rater variability. An illustrative example of bladder dimension measurement for the bladder control protocol is depicted in **Figure 2A** for pCT image acquisition and **Figure 2B** for MR image acquisition.

1. Computed Tomography Image Generation

A CT image with a 2 mm slice thickness was obtained for all prostate cancer patients using a 32-slice Big Bore RT CT scanner (Philips, Healthcare, Andover, MA, USA). The patients were placed in a supine position with a full bladder condition. Initially, a CT image was acquired for bladder dimension control as part of the protocol, using an exposure setting of 120 kV and 190 mAs. This image served as the reference for HU and dose comparisons.

2. Synthetic Computed Tomography Image Generation

The sCT image was reconstructed from the MRCAT solution sCT version 4.1 (Philips Healthcare, Finland) by acquiring the MR image from a 3.0 Tesla Ingenia MR-RT simulator (Philips N.V., Netherlands). A commercial MRCAT solution is developed to map voxel electron density information that relies on a dual-echo 3D mDIXON fast field echo (FFE) sequence for the sCT reconstruction with continuous HU (more detail is illustrated by[19]). In this study, the patient was positioned identically to the CT simulation process. The organ check (pre-sCT) protocol, a component of the pre-imaging protocol, generated images in three planes (comprising three images per plane: the first, middle, and last

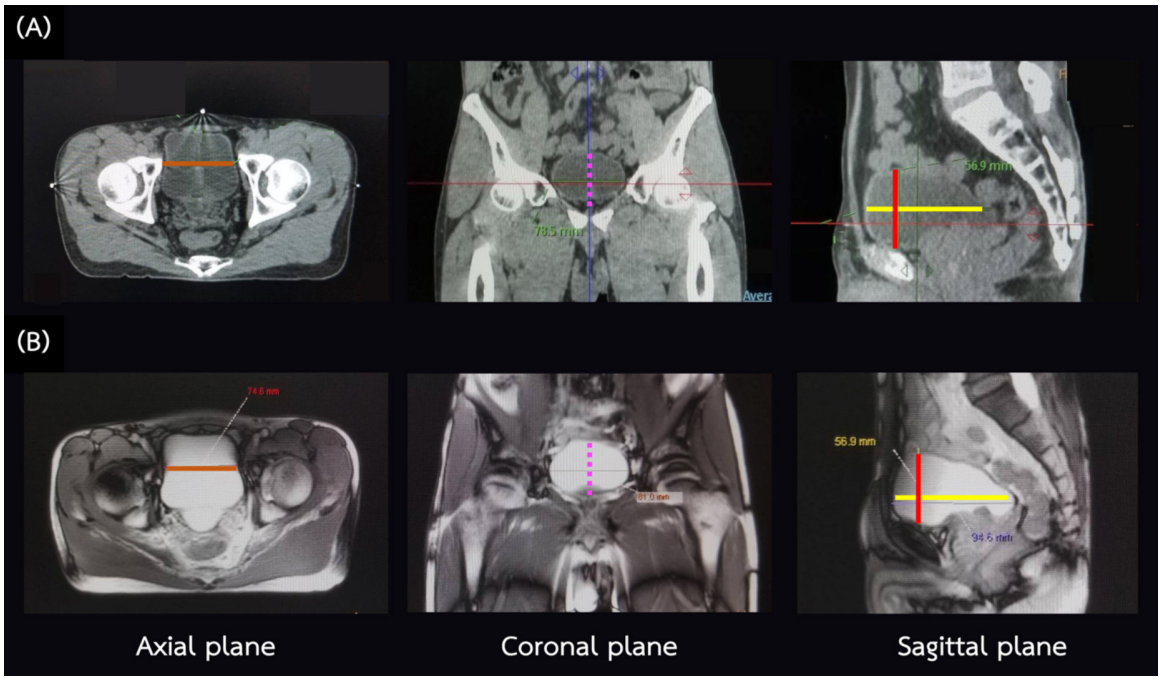

Figure 2. The bladder dimension control between two image scans. (A) Planning CT image with three planes was measured and used as a reference length for the MR scan. The brown line is the RL direction measured from right to left of the bladder wall, the yellow line is the AP direction measured from anterior to posterior of the bladder wall, the red line is the CC direction measured from mid-pubic symphysis to the bladder dome, and the pink dotted line is the height measured in some cases. (B) Pre-sCT images in each plane. Their lines were drawn as shown by the pCT to compare the bladder size at that moment.

images) embedded in the MR scanner to form the patient's body. Prior to sCT reconstruction, bladder dimensions were reevaluated using the planar image from each imaging plane. The resulting of sCT image was utilized for dose calculation in the planning process.

3. Magnetic Resonance Image Generation

T2-weighted (T2W) and diffusion-weighted imaging (DWI) with slice thicknesses of 1 and 3 mm were acquired for all prostate cancer patients in this prospective study. Both MR sequences were used for target and organs at risk (OARs) segmentation by experienced radiation oncologists (RO).

Contouring and Treatment Planning

Target and OARs for prostate cancer radiotherapy were delineated by more than 5-year experienced RO. The target structure, including the prostate gland and seminal vesicle, was delineated on the T2W MR image using the combination of the DWI image in the Eclipse treatment planning system version 16.1 (Varian Medical Systems, Palo Alto, CA). The target from the T2W image was transferred to the pCT and sCT by rigid registration with a local focus on the prostate region and expanded of 5 mm to generate the planning target volume (PTV). The accuracy of image registration between pCT and MR images was assessed by experienced RO based on a qualitative visualized check. In addition, the OARs, including the bowel, bladder, rectum, penile bulb, and femur, were segmented based on the pCT and sCT images. The average HU from individual OARs between the pCT and sCT was calculated and compared.

The 3-full arc of volumetric modulated arc therapy (VMAT) with 10 MV photons was generated based on the pCT image. The dose at the PTV was prescribed at 3 Gy per fraction in 20 fractions. The planning dose was calculated based on the Acuros XB (AXB) calculation algorithm using a 2 mm dose grid calculation. The treatment plan from the pCT image was transferred to the sCT image, and then the planning dose was recalculated by a similar dose calculation protocol.

Dose Similarity Evaluation

This study assessed the feasibility of sCT-based external beam dose calculations by evaluating specific dosimetric parameters extracted from the dose-volume histogram (DVH) of each relevant contour within the PTV and OARs. These parameters were derived from internal institutional clinical guidelines based on the definitive hypofractionation EBRT protocol for prostate adenocarcinoma, as outlined in **Table 1** for prostate plan evaluation[20]. In addition, the similarity of dose distribution between the dose calculated based on the sCT and pCT will be evaluated by considering the 3D gamma analysis (various gamma criteria from 3%3mm, 2%/2 mm, and 1%/1 mm with 10% dose threshold) on PTW-Verisoft software (PTW, Freiburg, Germany).

Statistical Analysis

The dimensions and volume of the bladder and the dose difference between the pCT and sCT-based dose calculations were considered by paired t-test or Wilcoxon Signed Rank test with a 95% confidence interval using IBM SPSS Statistics version 18 (IBM SPSS Statistics). The significant difference was considered at 0.05 ($p<0.05$).

Table 1. Dosimetric parameters for plan evaluation.

Structures	Prostate gland	PTV	Bowel	Bladder	Rectum	Penile bulb	Femurs
Dosimetric parameters	V_{60Gy}	D_{1cc}, $D_{(95\%)}$	V^{45Gy}, V_{15Gy}	V_{60Gy}, $V_{48.6Gy}$, $V_{40.8Gy}$	V_{60Gy}, V_{57Gy}, V_{46Gy}, V_{37Gy}	V_{40Gy}	$V_{(50\%)}$

Abbreriation: PTV: Planning target volume, Vx Gy: Percent of volume received absorbed dose x Gy, D_(x cc): Absolute dose coverage at a RT structure volume of x cc.

Results

Image Characteristics and Contours zEvaluation

Dimensions and Volume of Bladder in Pre-imaging Protocol

The mean difference in the bladder length in all directions from the pre-imaging procedure between CT and MR was -0.22±0.53 cm. The mean length of the bladder in the CT image was relatively shorter than MR in RL and CC directions (7.36 cm and 5.15 cm for CT, and 7.64 cm and 5.19 cm for MR, respectively), while the length of the bladder in the CT image was greater in the AP direction (8.06 cm for CT and 7.76 cm for MR). This study was not found a significant different in bladder length between CT and MR. However, the mean volume of the bladder on the sCT was significantly larger than the pCT, at around 10.83±13.78 $cm^{[3]}$ ($p<0.05$). The bladder volume ratio between the sCT and pCT ranged from 0.92 to 1.32. The result of bladder control of pre-imaging in each patient is shown in **Table 2**.

Hounsfield Unit of Interested Contours

This study found a low variation of HU for the inter-patients (10 patients) in the prostate gland, PTV, bowel, bladder, rectum, and penile bulb, whereas a high variation of HU was found in the femur. A small mean difference of HU between the pCT and the sCT was found in soft tissue (13.02±15.58 HU) and the smallest in the bladder at about 2.83±5.60 HU. Nonetheless, a considerable difference in HU was observed in the femurs of around 51.59±49.08 HU. Interestingly, a high variation of HU was found in the femur, while a slight variation was observed in soft tissue. The average HU extracted from the interested contours of each patient in the cohort is shown in **Figure 3**.

Dose Similarity Analysis

Dosimetric Analysis of Synthetic Computed Tomography

Our study found an insignificant difference in dosimetric parameters extracted from interested

Table 2. The length of bladder in all dimensions and volume measured during pre-imaging preparation of CT and MR images.

Number	Dimension (cm)									Volume (cm3)			
	RL			CC			AP						
	pCT	Pre-sCT	Δ Distance*	pCT	Pre-sCT	Δ Distance	pCT	Pre-sCT	Δ Distance	pCT	sCT	Ratio (sCT/pCT) (sCT/pCT)	% Difference**
1	7.17	7.46	0.29	5.69	5.69	0.00	8.79	9.46	0.67	207.30	270.10	1.30	30.29
2	7.48	8.35	-0.87	6.73	6.82	-0.09	7.82	7.54	-0.28	283.10	296.40	1.05	4.70
3	7.74	8.46	-0.72	2.88	3.48	-0.60	8.40	8.31	-0.09	108.50	131.00	1.21	20.74
4	8.49	7.72	0.77	6.47	6.33	0.14	6.65	4.04	-2.61	276.70	267.90	0.97	-3.18
5	8.25	8.07	0.18	5.34	4.60	0.74	9.45	9.21	-0.24	243.30	257.30	1.06	5.75
6	6.87	7.72	-0.85	4.05	4.73	-0.68	6.67	7.65	0.98	121.70	118.70	0.98	-2.47
7	6.93	7.29	-0.36	3.25	3.26	-0.01	7.84	7.08	-0.76	139.60	183.60	1.32	31.52
8	8.76	8.83	-0.07	7.09	6.79	0.30	6.67	6.88	0.21	265.90	245.50	0.92	-7.67
9	5.53	5.73	-0.20	4.55	5.06	-0.51	10.53	10.48	-0.05	199.50	228.70	1.15	14.64
10	6.40	6.73	-0.33	5.42	5.14	0.28	7.73	6.91	-0.82	182.70	208.20	1.14	13.96
Mean ± S.D.	7.36 ± 1.00	7.64 ± 0.91	-0.22 ± 0.53	5.15 ± 1.44	5.19 ± 1.25	-0.04 ± 0.45	8.06 ± 1.28	7.76 ± 1.78	-0.30 ± 0.99	202.83 ± 64.49	220.74 ± 60.00	1.11 ± 0.14	10.83 ± 13.78
P-value		0.116			0.768			0.363			<0.05		

* Δ Distance = $\text{Dimension}_{\text{pCT}} - \text{Dimension}_{\text{Pre-sCT}}$, the pre-sCT involved planar images used to reevaluate the dimensions of the bladder before the sCT generation.

** % Difference = $\frac{\text{Volume}_{\text{sCT}} - \text{Volume}_{\text{pCT}}}{\text{Volume}_{\text{pCT}}} \times 100$

*** Statistical difference at $p<0.05$

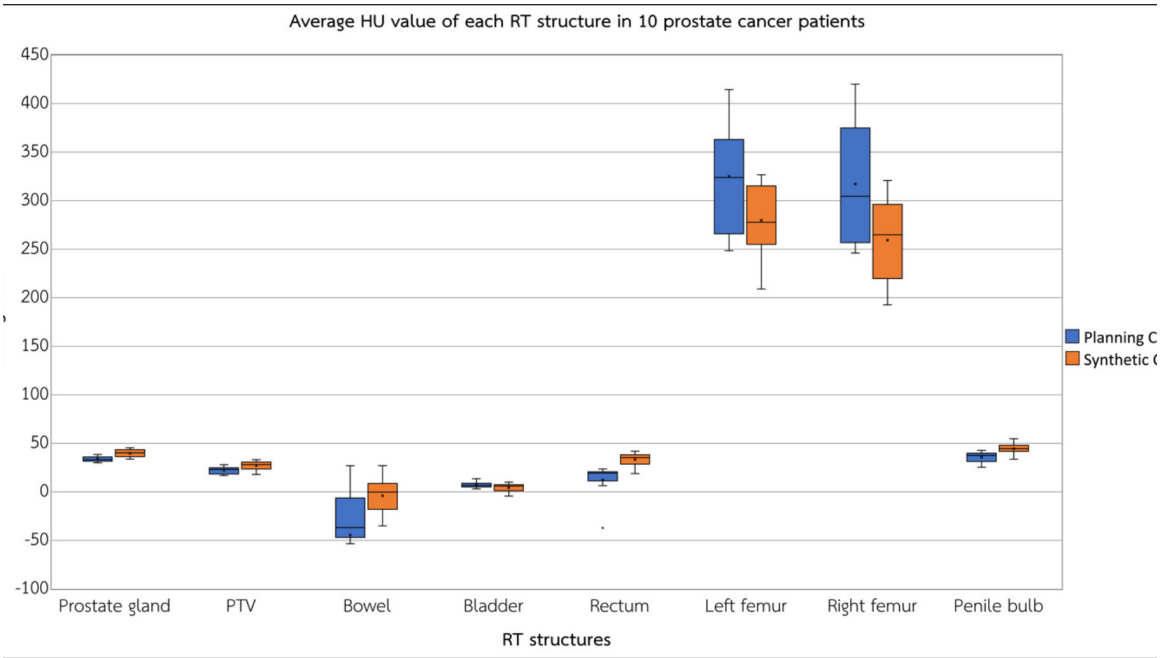

Figure 3. Average HU values comparison of each RT structure in 10 prostate cancer patients.

contours between the sCT and pCT except D95% of the PTV. The difference in dosimetric parameters between the sCT- and pCT-based dose calculations in the PTV was less than 0.2 Gy when considering D95% and D1cc, as well as less than 0.1% for V60Gy of the prostate gland. An inconsiderable volume difference percentage was observed in the OARs. However, the OARs dose from the sCT-based dose calculation was slightly higher than the pCT-based dose, especially at the parameter reflecting volume received high dose, e.g., 0.85% at V46Gy in the rectum. The results of the dose difference from our clinical dosimetric parameters between the pCT- and sCT-based dose calculations in the individual patients are summarized in **Table 3**.

Dose Distribution Analysis of Synthetic Computed Tomography

High similarity of 3D dose distribution between the pCT-based and sCT-based dose calculations was found in this study. The mean gamma passing rate was 99.9±0.2% when considering the 3%3mm gamma criteria, and it was reduced to 98.9±0.8% at the 1%1mm criteria. A slight difference in gamma analysis was observed in the high gradient dose of the PTV boundary, while a significant difference was found at the edge of the external body contour (**Figure 4**). The gamma passing rate of individual patients from this study is shown in **Table 4**.

Table 3. The mean±SD and range of percentage dose difference in the dosimetric parameters of RT structures from DVH comparing the pCT and sCT in 15 prostate cancer patients.

RT structure	Parameter	Mean±SD			p-value
		pCT	sCT	Absolute Difference*	
Prostate gland					
	V_60Gy(%)	100.00±0.00	99.94±0.13	-0.06±0.13	<0.05
PTV					
	D_1cc (Gy)	62.93±0.17	63.06±0.36	0.13±0.36	0.386
	D_(95%)(Gy)	60.57±0.10	60.41±0.17	-0.16±0.12	<0.05
Bowel					
	V_45Gy(%)	0.00±0.00	0.00±0.00	0.00±0.00	1.000
	V_15Gy(%)	0.29±0.92	0.10±0.32	-0.19±0.60	0.317
Bladder					
	V_60Gy(%)	3.59±2.29	3.51±1.65	-0.08±1.14	0.683
	V_48.6Gy(%)	9.18±4.94	9.33±4.06	0.15±1.90	0.575
	V_40.8Gy(%)	13.18±6.87	13.18±5.90	0.19±2.48	0.575
Rectum					
	V_60Gy(%)	2.85±2.08	3.60±2.76	0.74±2.87	0.386
	V_57Gy(%)	5.58±2.91	6.38±3.42	0.80±3.17	0.508
	V_46Gy(%)	12.46±4.24	13.31±4.62	0.85±3.66	0.445
	V_37Gy(%)	19.43±4.81	20.18±5.19	0.75±3.78	0.646
Penile bulb					
	V_40Gy(%)	16.39±30.03	16.24±29.12	-0.15±1.40	1.000
Left femur					
	V_(50%)(%)	0.06±0.12	0.05±0.12	-0.01±0.05	0.197
Right femur					
	V_(50%)(%)	0.39±0.89	0.02±0.04	-0.37±0.86	0.285

* Absolute difference: sCT - pCT

** $p<0.05$ was as statistical difference

Abbreriation: PTV: Planning target volume, $V_{x\,Gy}$: Percent of volume received absorbed dose x Gy, $D_{x\,cc}$: Absolute dose coverage at a RT structure volume of x cc, $D_{x\,\%}$: Absolute dose coverage at a RT structure volume of x %

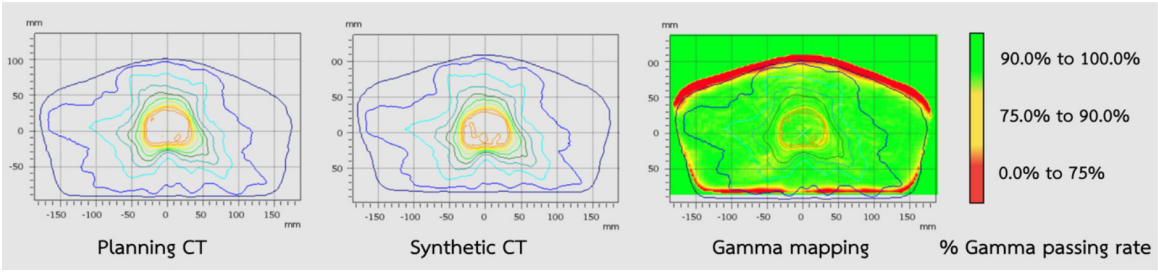

Figure 4. An example of the gamma analysis of one patient considered at the 3%/3mm criteria by comparing the pCT and sCT-based dose distributions. The color bar on the right displays the gamma passing rate results, with red indicating 0-75%, yellow representing 75-90%,
and green signifying scores above 90%.

Table 4. Dose distribution comparison between the pCT and sCT-based planning in prostate cancer patients based on a 3D gamma analysis.

Patient No.	Global Gamma Passing Rate (%)		
	3%/3mm	2%/2mm	1%/1mm
1	100.0	100.0	99.4
2	99.7	99.1	97.0
3	99.9	99.9	99.2
4	99.8	99.6	98.1
5	100.0	99.9	99.4
6	100.0	99.9	99.2
7	99.9	99.8	99.6
8	100.0	100.0	99.4
9	99.7	99.5	98.7
10	99.5	99.4	99.0
Mean±SD	99.9±0.2	99.7±0.3	98.9±0.8

Discussion

This study demonstrated the feasibility of the sCT generated from the MRCAT for prostate treatment plans, focusing on prospective clinical patients. The MRCAT is a commercially available tool for generating sCT images that rely on MR images. Thus, it allows patients to potentially reduce their exposure to ionizing radiation during CT scans. The accuracy of sCT images depends on the MRCAT generation method, which relies on voxel intensity in the source MRCAT in-phase and water-only images for body outline and bone creation through model-based segmentation. The voxel intensity in the source MRCAT fat and water-only images was utilized for tissue classification. These images were acquired through a 3D dual mDixon FFE sequence and were subsequently automatically converted to HU. The findings of this study indicated no major differences in the mean HU of soft tissue and bone. The disparity of HU between the values obtained from the sCT compared to the pCT was found to be larger in soft tissue. In contrast, the derived HU from the sCT and the pCT was smaller in bone. Consequently, a minor dosimetric difference in all interested contours and a highly similar dose distribution were observed between the pCT and the sCT. The significant dosimetric difference, e.g., D95% in the PTV, did not seem to be impacted by clinical meaning because the absolute dose difference was around 0.2 Gy.

Although this study found a slight difference in HU between the pCT and sCT, the HU in the bone region still had a high variation compared to soft tissue. The sCT generated from MR images exhibited poor capability in producing MR images from the bony region, which contains small amounts of hydrogen, which affects bone reconstruction in the sCT[21]. The largest difference of HU in the bone region at around a factor of 2 compared to the acceptable level of HU difference from a previous study (±20 HU and ±50 HU for soft tissue and bone, respectively) was observed in this study. The variation of HU within the recommended margin resulted in a dose change of less than 1% of the expected dose[22]. However, some studies showed that the difference in HU between the pCT and sCT in the femurs could be up to a factor of 3, which was higher than our discovery[23].

The observation of dose similarity between the pCT and sCT in this study closely aligns with many previous MRCAT studies in the pelvis region[11, 24-26]. Likewise, the trend of dose coverage to the PTV in the sCT was around 1% lower than the pCT when considering D95% or D98%. Nonetheless, a high dose in a small volume of the PTV and OARs tends to be increased by roughly 5% in the sCT compared to the pCT. By using the sCT generated from MRCAT, the HU on the image is a continuous value, which is different from other MR-based dose calculation techniques, e.g., the homoge-

nous HU in bulk density technique. Thus, applying a different dose calculation algorithm could potentially impact the dose distribution pattern[27]. This study applied AXB for treatment dose calculation to reduce dose calculation uncertainty from heterogeneous materials. However, this study considers the effect of the sCT only on the planning dose, and it is mandatory to compare the planning dose with the delivery dose before implementing the sCT in the clinic. The dose calculated from the sCT is not reflected in the actual patient dose as it could vary between inter-fractions[28].

The strengths of this study include the application of a dose calculation algorithm with corrective heterogeneity for soft tissue, specifically the AXB algorithm, which was known for its heightened sensitivity to HU changes[29]. The results clearly demonstrated discernible dose differences within each evaluated contour and the study also recruited prospective patients who underwent both pCT and MR images within the same day. This study controlled organ volume similarity between pCT and MR images by applying a water-controlling protocol with the pre-image dimension measurement for the bladder. In contrast, other studies only focus on the amount of water and waiting time without the dimension measurement[11, 24]. Nevertheless, the body outline is an alternative factor that has impacted dose distribution as it could change the depth of the ionization path. This effect is an unavoidable factor when patient repositioning from pCT to MR acquisition is required. As a result, the dose difference was experienced on the skin around the body; this effect was also found in other studies[11].

The limitation of this study was the difference in each individual patient's characteristics and behavior as it affected the organ dislocation between pCT and MR images. Even though our study implements the pre-image dimension measurement, it still found that some patients could not be tolerated when making a second attempt of the full bladder. Therefore, a marginal difference in bladder dimension and volume was observed. In addition, the air in the rectum and the rectum volume affected the PTV location, and in turn affected dose calculation. Also, a small volume of air in the rectum could potentially lead to an incorrect HU on the sCT, but it did not significantly impact the dose distribution pattern in this study. Although the sCT has been applied clinically in several institutions, to replace the pCT completely, for example, in the contouring process, further image quality analysis, such as image contrast and distortion, is still required[7, 30].

Conclusion

The use of the sCT image generated from MRCAT is feasible for prostate EBRT dose calculation. A slight difference in HU between the sCT and pCT was observed in soft tissue with a small HU variation, but a considerable difference was found in bone. The pCT and sCT

had similar dose distributions and negligible dosimetric differences in all contours. The result of this study provides a good promotion for the MR-only workflow in prostate EBRT.

Acknowledgements

There was no funding for this study. This work was approved by the Siriraj Institutional Review Board (SIRB protocol No. 039/2565). The authors appreciate and thank all the patients for participating in this research. The authors would like to thank Assoc. Prof. Lalida Tuntipumiamorn, and other supporting staff, Siriraj Hospital, Bangkok, for their assistance and excellent advice in ensuring the success of this endeavor. Finally, I would also like to thank Siriraj Graduate Scholarship.

References

1. Engeler CE, Wasserman NF, Zhang G. Preoperative assessment of prostatic carcinoma by computerized tomography. Weaknesses and new perspectives. Urol 1992;40:346-50.
2. Rasch C, Barillot I, Remeijer P, Touw A, van Herk M, Lebesque JV. Definition of the prostate in CT and MRI: a multi-observer study. Int J Radiat Oncol Biol Phys 1999;43:57-66.
3. den Hartogh MD, Philippens MEP, van Dam IE, Kleynen CE, Tersteeg RJHA, Pijnappel RM, et al. MRI and CT imaging for preoperative target volume delineation in breast-conserving therapy. Radiat Oncol 2014;9:63.
4. Platt JF, Bree RL, Schwab RE. The accuracy of CT in the staging of carcinoma of the prostate. Am J Roentgenol 1987;149:315-8.
5. Claus FG, Hricak H, Hattery RR. Pretreatment evaluation of prostate cancer: role of MR imaging and 1H MR spectroscopy. Radiographics 2004;24 Suppl 1:S167-80.
6. Turkbey B, Albert PS, Kurdziel K, Choyke PL. Imaging localized prostate cancer: current approaches and new developments. Am J Roentgenol 2009;192: 1471-80.
7. Tyagi N, Fontenla S, Zelefsky M, Chong TM, Ostergren K, Shah N, et al. Clinical workflow for MR-only simulation and planning in prostate. Radiat Oncol 2017; 12:119.
8. Goudschaal K, Beeksma F, Boon M, Bijveld M, Visser J, Hinnen K, et al. Accuracy of an MR-only workflow for prostate radiotherapy using semi-automatically burned-in fiducial markers. Radiat Oncol 2021;16:37-49.

9. Nierer L, Eze C, da Silva Mendes V, Braun J, Thum P, von Bestenbostel R, et al. Dosimetric benefit of MR-guided online adaptive radiotherapy in different tumor entities: liver, lung, abdominal lymph nodes, pancreas and prostate. Radiat Oncol 2022;17:53-66.
10. Chen L, Price RA, Jr., Nguyen TB, Wang L, Li JS, Qin L, et al. Dosimetric evaluation of MRI-based treatment planning for prostate cancer. Phys Med Biol 2004;49:5157-70.
11. Christiansen RL, Jensen HR, Brink C. Magnetic resonance only workflow and validation of dose calculations for radiotherapy of prostate cancer. Acta Oncol 2017;56:787-91.
12. Jonsson JH, Karlsson MG, Karlsson M, Nyholm T. Treatment planning using MRI data: an analysis of the dose calculation accuracy for different treatment regions. Radiat Oncol 2010;5:62-9.
13. Dowling JA, Sun J, Pichler P, Rivest-Hénault D, Ghose S, Richardson H, et al. Automatic Substitute Computed Tomography Generation and Contouring for Magnetic Resonance Imaging (MRI)-Alone External Beam Radiation Therapy From Standard MRI Sequences. International Journal of Radiation Oncology Biology Physics 2015;93 1144-53.
14. Johnstone E, Wyatt JJ, Henry AM, Short SC, Sebag-Montefiore D, Murray L, et al. Systematic Review of Synthetic Computed Tomography Generation Methodologies for Use in Magnetic Resonance Imaging-Only Radiation Therapy. Int J Radiat Oncol Biol Phys 2018;100:199-217.
15. Rank CM, Tremmel C, Hünemohr N, Nagel AM, Jäkel O, Greilich S. MRI-based treatment plan simulation and adaptation for ion radiotherapy using a classification-based approach. Radiat Oncol 2013;8:51-63.
16. Nyholm T, Nyberg M, Karlsson MG, Karlsson M. Systematisation of spatial uncertainties for comparison between a MR and a CT-based radiotherapy workflow for prostate treatments. Radiat Oncol 2009;4:54-62.
17. Dean CJ, Sykes JR, Cooper RA, Hatfield P, Carey B, Swift S, et al. An evaluation of four CT-MRI co-registration techniques for radiotherapy treatment planning of prone rectal cancer patients. Br J Radiol 2012;85:61-8.
18. Korsager AS, Carl J, Riis Østergaard L. Comparison of manual and automatic MR-CT registration for radiotherapy of prostate cancer. J Appl Clin Med Phys 2016;17:294-303.

19. Köhler M, Vaara T, Grootel Mv, Hoogeveen RM, Kemppainen R, Renisch S, editors. MR-only simulation for radiotherapyn planning White paper: Philips MRCAT for prostate dose calculations using only MRI data. 2015.
20. eviQ. Prostate adenocarcinoma definitive EBRT hypofractionation: Cancer Institute NSW; 2018 [updated 30 Dec 2021; cited 2023 8 Aug]. Available from: https://www.eviq.org.au/p/3370.
21. Aisen AM, Martel W, Braunstein EM, McMillin KI, Phillips WA, Kling TF. MRI and CT evaluation of primary bone and soft-tissue tumors. Am J Roentgenol 1986; 146:749-56.
22. Davis AT, Palmer AL, Nisbet A. Can CT scan protocols used for radiotherapy treatment planning be adjusted to optimize image quality and patient dose? A systematic review. Br J Radiol 2017;90:20160406.
23. Farjam R, Tyagi N, Deasy JO, Hunt MA. Dosimetric evaluation of an atlas-based synthetic CT generation approach for MR-only radiotherapy of pelvis anatomy. J Appl Clin Med Phys 2019;20:101-9.
24. Kemppainen R, Suilamo S, Tuokkola T, Lindholm P, Deppe MH, Keyrilainen J. Magnetic resonance-only simulation and dose calculation in external beam radiation therapy: a feasibility study for pelvic cancers. Acta Oncol 2017;56: 792-8.
25. Tyagi N, Fontenla S, Zhang J, Cloutier M, Kadbi M, Mechalakos J, et al. Dosimetric and workflow evaluation of first commercial synthetic CT software for clinical use in pelvis. Phys Med Biol 2017;62:2961-75.
26. Bratova I, Paluska P, Grepl J, Sykorova P, Jansa J, Hodek M, et al. Validation of dose distribution computation on sCT images generated from MRI scans by Philips MRCAT. Rep Pract Oncol Radiother 2019;24:245-50.
27. Yan C, Combine AG, Bednarz G, Lalonde RJ, Hu B, Dickens K, et al. Clinical implementation and evaluation of the Acuros dose calculation algorithm. J Appl Clin Med Phys 2017;18:195-209.
28. Buranaporn P, Dankulchai P, Jaikuna T, Prasartseree T. Relation between DIR recalculated dose based CBCT and GI and GU toxicity in postoperative prostate cancer patients treated with VMAT. Radiother Oncol 2021;157:8-14.
29. Bouyer C, Fargier-Voiron M, Beneux A. Comparison of algorithms AAA and Acuros (AxB) on heterogenous medium. Physica Medica 2017;44:286-91.
30. Kerkmeijer LGW, Maspero M, Meijer GJ, van der Voort van Zyp JRN, de Boer HCJ, et al. Magnetic resonance imaging only workflow for radiotherapy simulation and planning in prostate cancer. Clin Oncol 2018;30:692-701.